Available online at www.sciencedirect.com
SCIENCE DIRECT®
Journal of Catalysis 222 (2004) 192–206
JOURNAL OF CATALYSIS
www.elsevier.com/locate/jcat

Comparative isotope-aided investigation of electrochemical promotion and metal–support interactions 1. $^{18}O_2$ TPD of electropromoted Pt films deposited on YSZ and of dispersed Pt/YSZ catalysts

A. Katsaounis, Z. Nikopoulou, X.E. Verykios, and C.G. Vayenas *

Department of Chemical Engineering, 1, Caratheodory St., University of Patras, GR-26504 Patras, Greece

Received 25 July 2003; revised 10 October 2003; accepted 14 October 2003

Abstract

The adsorption of $^{18}O_2$ on porous electropromoted Pt films deposited on Y_2O_3-stabilized ZrO_2 (YSZ) and on nanodispersed Pt catalysts deposited on YSZ powder was investigated via TPD. The TPD spectra are very similar for both systems: When $^{18}O_2$ adsorption takes place above 200 °C, two O adsorption states (β_2 and β_3 states) form, which desorb at 425 and 500 °C, respectively. The latter is always occupied by lattice oxygen. For $^{18}O_2$ adsorption temperatures below 100 °C a weakly bonded state (β_1 state) forms in addition to the β_2 and β_3 states. It desorbs at 100–160 °C and is occupied exclusively by ^{18}O. Both the Pt film and the nanodispersed Pt catalyst act as oxygen portholes and mediate, via O spillover and backspillover, respectively, the incorporation of gaseous $^{18}O_2$ into the YSZ lattice during adsorption as well as the desorption of lattice ^{16}O during TPD. The excess oxygen stored in YSZ plays a key role in interpreting the TPD spectra. The observed very strong similarity between the O_2 TPD spectra of electrochemically promoted Pt/YSZ films and nanodispersed Pt/YSZ powder catalysts corroborates the mechanistic equivalence of electrochemical promotion and metal–support interactions (MSI) with O^{2-}-conducting supports.

Keywords: Temperature-programmed desorption; Oxygen on Pt; Oxygen adsorption; Platinum–YSZ catalysts; Electrochemical promotion; TPD; Metal–support interactions; Spillover–backspillover of oxygen; Yttria-stabilized ZrO_2 (YSZ); Catalyst support; NEMCA effect; Platinum catalysts; YSZ supported

1. Introduction

Electrochemical promotion of catalysis [1–15] and metal–support interactions with ionically conducting (Y_2O_3-stabilized ZrO_2, YSZ) or mixed ionic–electronic conductors (ZrO_2, CeO_2, TiO_2, W^{6+}-doped TiO_2) [15–25] are phenomena which both affect the chemisorptive and catalytic properties of metal catalysts in a very profound manner.

In the case of electrochemical promotion (EPOC or NEMCA effect) the metal catalyst is usually in the form of a porous and electronically conducting film deposited on the solid electrolyte (e.g., O^{2-} or mixed O^{2-}-electronic conductor) while in the case of metal–support interactions (MSI) the metal is in the form of nanoparticles deposited on the porous O^{2-} or mixed O^{2-}-electronic conducting support.

It has been recently shown via several techniques [15, 26–29] including STM [27] that the two phenomena are closely related and mechanistically equivalent as they both stem from the migration (reverse spillover) of anionic $O^{\delta-}$ species from the support to the metal–gas interface. These backspillover $O^{\delta-}$ species together with their image charge in the metal create an overall neutral double layer at the metal–gas interface and thus affect both chemisorption and catalysis at this interface in a pronounced manner. At high oxygen coverages the backspillover $O^{\delta-}$ species are distinct from, and more strongly adsorbed than, oxygen adsorbed from the gas phase. They are also less reactive for catalytic oxidations than gas-supplied oxygen and thus act as sacrificial promoters [14,15]. The backspillover is thermal in the case of MSI and electrochemically assisted in the case of NEMCA [14,15,26,30], as shown in the latter case by numerous surface spectroscopic (XPS, UPS, TPD, STM) and electrochemical (AC impedance, cyclic voltammetry) techniques [15,26–30].

* Corresponding author.
E-mail address: cat@chemeng.upatras.gr (C.G. Vayenas).

0021-9517/$ – see front matter
doi:10.1016/j.jcat.2003.10.010

The purpose of the present work is to use isotopic oxygen, $^{18}O_2$, chemisorption in conjunction with temperature-programmed desorption (TPD) in order to test the above mechanistic equivalence for Pt films deposited on YSZ disks and for nanodispersed Pt deposited on YSZ powder catalysts.

The chemisorption of O_2 on Pt single crystal surfaces [31–43] and polycrystalline samples [44–47] is one of the most thoroughly studied problems in surface science. It is well established via TPD that molecular O_2 states, termed α-states, desorb below −70 °C while atomically adsorbed O (β states) desorb at temperatures of 420 to 650 °C. Subsurface "oxide" oxygen desorbs above 1000 °C. In addition to the above well-known states, very recently Huang et al. [48] have shown the creation of a weakly bonded atomic O state on Pt(110) during NO_2 decomposition which desorbs at temperatures below 400 °C.

There have been numerous TPD investigation of supported Pt catalysts (e.g., Pt/Al_2O_3, Pt/ZrO_2, Pt/CeO_2, Pt/TiO_2) but most of them address the chemisorption of other gases, such as CO, NO, N_2O, NH_3, and H_2 and relatively few of them address the chemisorption of O_2: Hwang and Yen [49] present O_2 TPD spectra from 5% Pt/γ-Al_2O_3 after O_2 exposure at 25, 300, and 500 °C and obtain a peak desorbing near 600 °C. These spectra, however, do not include the region below 300 °C. Similar is the case of the O_2 TPD spectra of Putna et al. obtained with Pt/α-Al_2O_3 [50]. Uner et al. [51] studied O_2 adsorption on Pt/TiO_2 at room temperature and found a pronounced decrease in the heat of adsorption (from 300 to 0 kJ/mol) upon increasing the surface O/Pt ratio from zero to 0.8. Primet and co-workers [52] have found evidence for a low-temperature desorbing oxygen state at 80 °C in addition to the two main β peaks at 450 and 550 °C with Pt/Al_2O_3 and Pt/Ba–Al_2O_3 catalysts.

Mitterdorfer and Gauckler [53] have investigated in detail the mechanism of O_2 reduction to O^{2-} on Pt/YSZ electrodes and found strong evidence for the existence of two oxygen species on the Pt electrode surface and for the formation of an effective double layer at the electrode/gas interface due to the backspillover of $O^{\delta-}$, in agreement with the electrochemical promotion literature [15,26–30].

There is a rich literature on the oxygen-storage capacity of CeO_2 and CeO_2–ZrO_2 supports [54–57] as well as for isotopic oxygen exchange on YSZ surfaces [58–60]. These studies are quite relevant to the present work as shown below.

Oxygen TPD has been used to investigate the mechanism of electrochemical promotion on Pt/YSZ films using O_2 adsorption temperatures above 200 °C [45–47]. In addition to the β state desorbing at 420 to 450 °C (labeled in the present work β_2 state), a second β state (labeled in the present work β_3 state) desorbing at 500 to 520 °C was found to form upon electrochemical O^{2-} supply to the Pt film.

To the best of our knowledge there have been no previous $^{18}O_2$ TPD studies of Pt/YSZ films and supported Pt/YSZ powder catalysts. Au-Yeung et al. [61] have used $^{18}O_2$ to study the dynamics of oxygen exchange between pure ZrO_2 and PdO. The use of $^{18}O_2$ adsorption allows for direct differentiation among lattice oxygen, ^{16}O, and gaseous supplied oxygen ^{18}O.

2. Experimental

2.1. Preparation and characterization of model electrochemically promoted catalysts (Pt film deposited on YSZ)

The gold reference and counterelectrodes (Fig. 1) were deposited on one side of the YSZ disk (Dynamic–Ceramic; diameter 19 mm; thickness 2 mm) by application of a thin coating of Engelhard A-1118 Au paste and calcining in air at 400 °C for 2 h and then at 850 °C for 30 min. The catalyst (working electrode) consisted of a thin Pt film (Fig. 1) deposited on the other side of the YSZ disk using a thin coating of Engelhard A-1121 paste and calcining in air at 450 °C for 2 h and then at 700 °C for 30 min. The mass of the porous Pt film was 3.15 mg, its superficial surface area was 1 cm^2, and its thickness approximately 1.1 μm. Its true surface area, N_G, expressed in moles O, was measured via isothermal surface titration of C_2H_4 with O_2 at 370 °C [13,14] and via measurement of the relaxation time constant, τ, during galvanostatic electrochemical promotion experiments of C_2H_4 oxidation

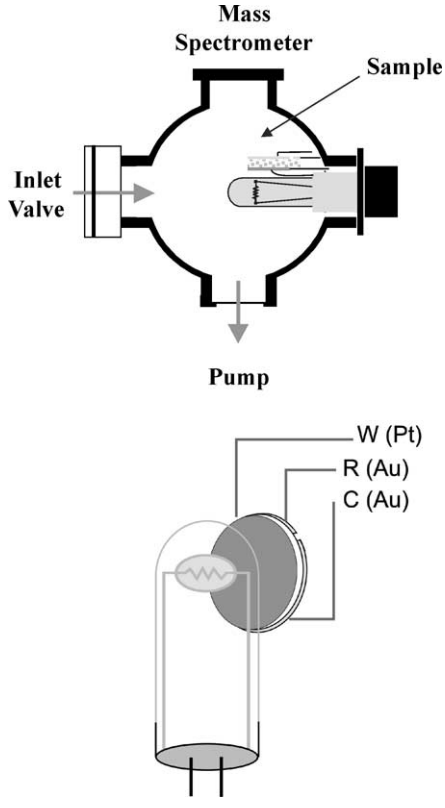

Fig. 1. Schematic of the UHV chamber and heating system used for TPD (top) and of the Pt film/YSZ disk sample with Au counter and reference electrodes (bottom).

at 370 °C using [13,14]

$$N_G = \tau I/2F. \quad (1)$$

Both techniques gave N_G values of 2.7×10^{-8} mol O (±30%). We have also used AC impedance spectroscopy to measure the capacitance of the metal–solid electrolyte interface, $C_{d,1}$, and of the metal–gas three-phase-boundaries, $C_{d,2}$, at 350 °C [14]. The measured values were 2.9×10^{-7} and 1.6×10^{-4} F, respectively. From these measurements one can estimate the reactive oxygen uptake, N_{tpb}, at the three-phase boundaries (tpb) using the following equation [14]:

$$\frac{N_{tpb}}{N_G} = \frac{C_{d,1}}{C_{d,2}}. \quad (2)$$

Thus from the measured C_d values, the above ratio is 1.8×10^{-3} and one obtains the value $N_{tpb} = 4.9 \times 10^{-11}$ mol O for the reactive oxygen uptake at the three-phase boundaries metal–YSZ–gas.

The final calcination temperature (700 °C here vs 800–850 °C in most previous electrochemical promotion studies, including the earlier TPD study [46]) is known to affect via sintering the porous Pt film surface area and tpb length, but not the surface cleanliness, since combustion of the organic precursor is completed after 2 h at 450 °C [13,14]. It is worth noting that, despite the lower present calcination temperature (700 °C vs 830 °C in [46]) the N_G value in the present work (2.7×10^{-8} mol O) is lower than that in Ref. [46] (2.0×10^{-7} mol O) due to the significantly lower total mass of the Pt film in the present study.

2.2. Preparation and characterization of supported nanodispersed Pt/YSZ catalyst (1% Pt/YSZ)

The dispersed Pt catalyst was prepared by the method of incipient wetness impregnation of ZrO_2 (8% Y_2O_3) powder (TOSOH–ZIRCONIA TZ-8Y) with an aqueous solution of $(NH_3)_2Pt(NO_2)_2$ (Alfa). Weighted amounts of the support material and the appropriate solution volume of the metal precursor, corresponding to 1 wt% Pt loading, were mixed under continuous stirring. The temperature was then slowly raised to 70–80 °C in order to evaporate the water and the residual slurry was dried at 110 °C for 24 h. The dried material was ground, sieved, heated in N_2 for 2 h at 300 °C to decompose the $(NH_3)_2Pt(NO_2)_2$ precursor [62] which is known to decompose quantitatively at 240 °C in N_2 [63], and finally reduced under flowing hydrogen at 300 °C for 2 h.

The Pt surface area was measured via H_2 chemisorption to be 1.8×10^{-5} mol Pt/g catalyst. This gives a Pt dispersion value of 0.35 (±20%). More details of the technique are given elsewhere [64]. The Pt dispersion was also measured after the He and H_2 thermal treatment preceding each TPD run described in the next section. The dispersion was found to remain practically constant.

2.3. TPD under UHV conditions

The experiments were carried out in an ultrahigh vacuum chamber (Fig. 1) (base pressure 10^{-10} Torr after baking) equipped with a quadrupole mass spectrometer (Balzers QMG 420) and a leak valve gas inlet system. The signal of the spectrometer was calibrated, using the Pt/YSZ/Au electrochemical cell, as described in Section 3, to give the desorption rate, dN/dt, in mol O/s. The sample was heated radiatively using an Osram xenon lamp located above the catalyst film. A type K thermocouple attached on the Pt surface (film of Pt/YSZ) or immersed in the powder catalyst sample (supported catalyst) was used to measure the temperature. The temperature could be varied linearly at a heating rate as high as 2 K/s using a Eurotherm programmable temperature controller. In the case of the model catalyst of Pt film deposited on YSZ, constant currents between the Pt film and the Au counterelectrode (galvanostatic operation) or constant potentials between the Pt film and the Au reference electrode (potentiostatic operation) were applied by an AMEL 553 galvanostat–potentiostat.

The oxygen adsorption for the case of the *supported catalyst* was carried out by exposure to $P_{^{18}O_2} = 10^{-7}$ mbar for various exposure times, $t_{^{18}O_2}$. The $^{18}O_2$ gas was introduced to the vacuum chamber through a leak valve. Three modes of oxygen adsorption were used in the case of the Pt/YSZ *film* at various adsorption temperatures, T_{ad}:

(1) Gaseous oxygen adsorption by exposure to $P_{^{18}O_2}$ of the order of 10^{-7} mbar for various exposure times, $t_{^{18}O_2}$, corresponding to several Langmuirs (1 L = 10^{-6} Torr s, 1 Torr = 1.33 mbar).
(2) Electrochemical oxygen supply ($^{16}O^{2-}$) at a rate $I/2F$ for various times, t_I, of positive current I application between the Pt film and the Au counterelectrode.
(3) Mixed gas and electrochemical adsorption. In this mode the film was first exposed to $P_{^{18}O_2}$ for time $t_{^{18}O_2}$, followed by an electrochemical supply of lattice oxygen ($^{16}O^{2-}$) through the solid electrolyte for a time t_I. In one set of experiments the inverse procedure was followed, i.e., electrochemical adsorption preceded gaseous adsorption as discussed in Section 3.

In both cases (Pt/YSZ film or supported catalyst 1% Pt/YSZ) after oxygen adsorption, the sample was cooled rapidly (1 min) under open circuit (to 50 °C for low-T adsorption and to 120 °C for high-T adsorption), followed by a linear increase in temperature at a heating rate β (K/s) *again under open circuit* in order to obtain the TPD spectra. The cooling time (1 min) was dictated by the time necessary for the sample to reach the desired initial temperature of the TPD run and not by the pumping time of the vacuum system which was much shorter. For the case of platinum film on YSZ a series of blank TPD experiments showed that the YSZ disk and the Au electrodes did not desorb any measurable amount of oxygen. Gold interfaced with YSZ has been found

to adsorb oxygen only upon anodic polarization as a working electrode [65], which corresponds to a cathodic cell operation in the present case (Au is the counterelectrode). Thus all the TPD spectra reported here can safely be attributed to oxygen desorption from the Pt film only. Both types of catalysts (Pt/YSZ film and supported Pt/YSZ powder) were cleaned in the vacuum system. The "cleanup" procedure includes the treatment of the surface with oxygen from the gas phase followed by temperature-programmed desorption. This resulted in a gradual increase of the amount of oxygen desorbing after a fixed oxygen dose. At the end of the cleanup treatment a reproducible oxygen desorption spectrum was achieved. Furthermore, no CO signal was detected during TPD, which is a good indication for the absence of carbon on the surface.

2.4. TPD under atmospheric pressure conditions

The reactor used for atmospheric pressure O_2 TPD consists of two 4.0 mm i.d. sections of quartz tubes which serve as inlet and outlet to and from a quartz cell of 7.0 mm i.d. (nominal volume 2 cm^3). The entrance to the reactor cell was machined in such a way as to create local gas mixing. Heating was provided by a small furnace controlled by a Eurotherm programmable temperature controller. The temperature of the catalyst sample was measured by a K-type thermocouple placed within a quartz capillary well in the middle of the catalyst bed. An appropriate flow system that allows for the application of transient methods (abrupt switches in the feed gas composition) was employed in the present investigation. The main design features of this system have been described in detail elsewhere [66]. The H_2 and He gases used were of ultrahigh purity (99.999%). Further purification of these gases was performed by using molecular sieve (13X) and MnO_x traps for removing traces of water and oxygen, respectively.

Analysis of the gases during transient experiments was done by on-line mass spectrometer (Fisons, SXP Elite 300H) equipped with a fast response inlet capillary/leak diaphragm system. Calibration of the mass spectrometer was performed based on prepared gas mixtures of known composition. The output signal from the mass spectrometer was then converted to ppm values. The integrity of the transient results, free of any flow disturbances caused by switching the chromatographic valves (use of electric actuators), was maintained as described elsewhere [66]. $^{18}O_2$, $^{16}O^{18}O$, $^{16}O_2$, and N_2 transients were recorded at $m/z = 36$, 34, 32, and 28, respectively.

The procedure of $^{18}O_2$ TPD on Pt-supported catalysts (1% Pt/YSZ) experiments was the following: The catalyst was first heated up to 650 °C under He flow. At this temperature the feed was switched to flowing H_2 and the sample was rapidly cooled to the desired temperature for adsorption. This thermal treatment was used to simulate the corresponding thermal treatment in vacuum of the Pt/YSZ film and powder samples during each TPD high-vacuum run. The maximum temperature of the treatment (650 °C) was chosen in order to avoid any loss of dispersion due to sintering in the reducing environment. As already noted, this treatment did not cause any measurable decrease in metal dispersion. After purging for 5 min with He, the feed was switched to a static gas atmosphere (200 kPa absolute pressure) containing a mixture of 1% $^{18}O_2$ in He mixture for 1 h. Finally, the catalyst was purged with flowing He for 2 min (He flow rate 40 cm^3 STP/min, free reactor volume ~ 1.6 cm^3) and the temperature was raised linearly ($\beta = 1.5$ K/s) in a He flow of 40 cc/min STP in order to obtain the TPD curves of $^{18}O_2$, $^{16}O^{18}O$, and $^{16}O_2$.

3. Results and discussion

3.1. $^{18}O_2$ adsorption on Pt/YSZ film

Fig. 2a shows O_2 TPD spectra from the Pt/YSZ film first *without* any gaseous $^{18}O_2$ adsorption (broken lines) and second (solid curves) after gaseous $^{18}O_2$ adsorption at 275 °C ($^{18}O_2$ exposure 2 kL, i.e., exposure to $p_{^{18}O_2} = 10^{-6}$ mbar for 45 min). In the latter case, Fig. 2a also shows the corresponding variation of the Pt film potential, U_{WR}, with respect to the reference electrode. Over wide temperature ranges the film potential is related to the work function, Φ, of the gas-exposed film surface via [1,13,14]

$$e\Delta U_{WR} = \Delta\Phi \tag{3}$$

so that the U_{WR} transient reflects the transient Φ behavior during the TPD run. In general, each O_2 desorption peak causes a significant decrease in U_{WR} and Φ as also shown in Fig. 2a.

In agreement with previous work [46], the first spectrum (broken lines) in Fig. 2a shows that, without any previous gaseous adsorption, no O_2 (i.e., $^{16}O_2$) desorption takes place from the Pt/YSZ film at temperatures below 550 °C.

The second set of TPD spectra (solid lines) shows, surprisingly, that the O_2 TPD broad peak at ~ 520 °C, also reported in our previous work [46], consists primarily from $^{16}O_2$, i.e., originates from *lattice oxygen*. Actually, as shown in Fig. 2a, one reason that this peak is so broad, is that it consists of three peaks, i.e., $^{18}O_2$ at $T_p = 425$ °C, $^{18}O^{16}O$ at 450 °C, and $^{16}O_2$ at 520 °C.

It is worth noting that there is significant isotopic oxygen scrambling, i.e., the $[^{16}O^{18}O]^2/[^{16}O_2][^{18}O_2]$ ratio increases with temperature during the TPD peak and approaches the value of four (complete scrambling) after the T_p peak maximum. Despite the isotope scrambling, it is clear that the lower desorption temperature peak (labeled hereafter state β_2 for reasons explained below) is heavily populated by ^{18}O while the higher desorption peak (labeled hereafter β_3) is populated predominantly by lattice oxygen ^{16}O.

This observation is not too surprising in view of previous O_2 TPD work of Pt/YSZ films under electrochemical promotion conditions [45–47], which has shown clearly that

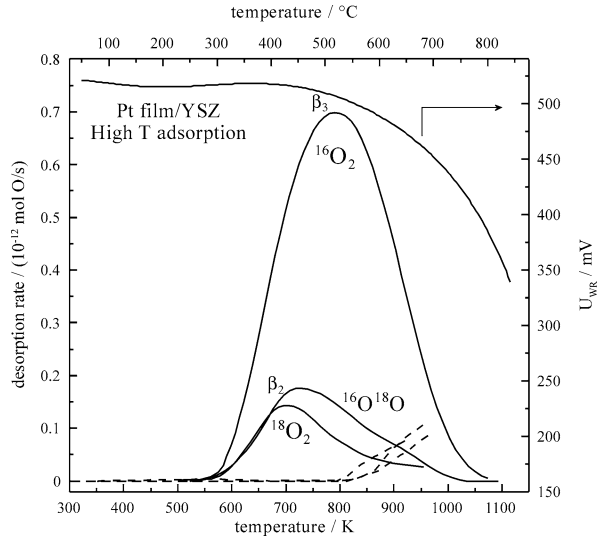

Fig. 2. (a) Pt/YSZ film, high-T adsorption: thermal desorption spectra of $^{18}O_2$, $^{16}O^{18}O$, and $^{16}O_2$ and corresponding catalyst potential, U_{WR}, variation after gaseous $^{18}O_2$ dosing of 2 kL ($P_{^{18}O_2} = 10^{-6}$ mbar for 45 min) at 275 °C. Dashed lines are spectra taken without any gaseous adsorption. Desorption was performed with a linear heating rate, $\beta = 0.5$ °C/s. (b) Pt/YSZ film, low-T adsorption: thermal desorption spectra after gaseous isotope oxygen dosing of 135 L ($P_{^{18}O_2} = 10^{-7}$ mbar for 30 min) at 70 °C. Dashed lines are spectra taken without any gaseous adsorption. Desorption was performed with a linear heating rate, $\beta = 0.5$ °C/s.

(as also discussed here in Section 4) under EPOC conditions (anodic polarization) two distinct O_2 desorption peaks appear, one at $T_p \approx 425$ °C corresponding primarily to gaseous supplied oxygen, the other at $T_p \approx 500$ °C corresponding to strongly bonded anionic oxygen electromigrating under anodic polarization from the YSZ solid electrolyte.

The spectra of Fig. 2a show that these two peaks (states β_2 and β_3) also exist under open-circuit conditions. This again is quite logical due to the thermal migration of O^{2-} from the YSZ lattice to the Pt surface and the establishment there of an effective double layer at temperatures above 300 °C as well documented in the literature on the basis of WF measurements [1] and several electrochemical and surface spectroscopic techniques [13,14]. This reverse spillover (also termed backspillover) of O^{2-} from the support to the metal/gas interface has been shown recently to be the origin of metal–support interactions for supports with finite O^{2-} mobility [14,26].

The most interesting, and at first not obvious, feature of Fig. 2a is that lattice oxygen ($^{16}O_2$) desorbs from the Pt/YSZ film only after the sample has been exposed to $^{18}O_2$. In fact, in order to cause $^{16}O_2$ desorption, this exposure to $^{18}O_2$ must take place at elevated oxygen adsorption temperature (e.g., $T_{ads} = 275$ °C as in Fig. 2a). When the exposure to $^{18}O_2$ takes place at lower temperatures (e.g., $T_{ads} = 70$ °C) the behavior is "normal"; i.e., only $^{18}O_2$ and no lattice O_2 ($^{16}O_2$) desorbs during the TPD run at temperatures below 540 °C as shown in Fig. 2b. The onset of high-temperature desorption ($T > 540$ °C) is the same as in the case of no previous $^{18}O_2$ adsorption (Fig. 2a, dashed lines) as also shown by the dashed lines in Fig. 2b. The presence of some ^{18}O in the high-temperature desorption area ($T > 540$ °C), even without immediate previous exposure to $^{18}O_2$, is due to repeated $^{18}O_2$ exposure in previous TPD runs.

The striking feature of Fig. 2b is, however, the appearance of a low-temperature $^{18}O_2$ desorption peak ($T_p \approx 157$ °C) in conjunction with the disappearance of the β_2 and β_3 peaks. The area of this low temperature $^{18}O_2$ desorption peak (1.7×10^{-11} mol O), labeled hereafter β_1 state, is roughly 3% of the O_2 desorbing as $^{18}O_2$, $^{18}O^{16}O$, or $^{16}O_2$ from states β_2 and β_3 in Fig. 2a (4.56×10^{-10} mol O).

As shown below, state β_1 appears also in the supported Pt/YSZ catalysts both in vacuum and in atmospheric pressure TPD carried out in a totally different apparatus, so it is certainly not due to any experimental artifact. Our TPR work utilizing $^{18}O_2$ for CO oxidation has shown that state β_1 is entirely responsible for the low-temperature oxidation activity of Pt/YSZ catalysts [67]. Yet, to the best of our knowledge, state β_1 has not been previously reported. It is reminiscent of the low-temperature state found by Primet and co-workers on Pt/Al_2O_3 catalysts [52], although in that study, where O_2 adsorption was performed at 500 °C, the peak was not isolated as is the case here. The peak observed by Huang et al. [48] on unsupported Pt, i.e., Pt(111), during NO_2 decomposition desorbs at 223 °C and is thus very probably not related to state β_1. We have found similar β_1 states for Pt/CeO_2, Pt/γ-Al_2O_3, Pt/TiO_2, and Pt/W^{6+}-doped TiO_2 catalysts [67]. As shown below, this state very probably corresponds to O adsorbed at the three-phase boundaries Pt–YSZ–gas.

As already noted, the first important feature of Fig. 2b is the disappearance of the β_2 and β_3 states and the onset of $^{16}O_2$ and some $^{18}O_2$ and $^{18}O^{16}O$ desorption at temperatures above 540 °C, similar to the case of no previous gaseous adsorption. It should be remembered that in Fig. 2b before gaseous O_2 adsorption at 70 °C the sample has been, as always, previously exposed to $T = 700$ °C in vacuum

during the preceding TPD run, and thus YSZ is partially oxygen deficient, i.e., has been depleted from nonstoichiometric oxygen, O(YSZ), as discussed below. Consequently the disappearance of the β_2 and β_3 peaks can be attributed to ^{16}O and ^{18}O spillover into the bulk of the oxygen-deficient YSZ during the TPD run, as also discussed below. Since the equilibrium concentration of O(YSZ) is a decreasing function of temperature for any fixed p_{O_2} value [68,69], including the vacuum system p_{O_2} value during the TPD run, it follows that the thermodynamic driving force for O spillover (into the bulk of the previously thermally equilibrated in vacuum at 700 °C oxygen-deficient YSZ) is larger than the driving force for O_2 desorption. Equivalently, the chemical potential of oxygen in the oxygen-deficient YSZ is lower than in the gas phase of the vacuum system for any T less than 700 °C. This can explain from a thermodynamic viewpoint the disappearance of states β_2 and β_3 during the TPD run.

3.2. Oxygen nonstoichiometry and storage capacity of YSZ

As already noted, the key for rationalizing Figs. 2a and 2b, which, as shown in the present work, are characteristic of the interaction of gaseous O_2 with Pt/YSZ systems (both films and nanodispersed catalysts) is to remember that YSZ is a nonstoichiometric compound [14,68,69].

The O nonstoichiometry, $\delta_{O(YSZ)}$, is small, i.e., on the order of 10^{-5} and temperature dependent [68,69], but nevertheless sufficiently large to provide enough oxygen to form effective double layers on porous metal films deposited on YSZ without any significant change in the YSZ stoichiometry [14,68,69]. Thus, for the YSZ sample used in the present investigation ($m = 3.125$ g and $m_{Pt} = 3.15$ mg) and taking $\delta_{O(YSZ)} = 10^{-5}$, the excess O in the sample, hereafter denoted O(YSZ), is 4.95×10^{-7} mol O, i.e., sufficient to form, via O backspillover, 18 monolayers of O on the Pt surface, which has a reactive oxygen uptake, N_G, of 2.7×10^{-8} mol. When YSZ is depleted from excess nonstoichiometric O, then YSZ can also easily absorb oxygen adsorbed on the Pt surface via oxygen spillover.

This is demonstrated in Fig. 3a which shows the variation in the MS signal of O_2 at mass 32 in the vacuum system and concomitant variation in O_2 desorption rate upon application of constant anodic currents ($I = 1$ to 20 μA) to a Pt/YSZ/Au cell at 375 °C. The MS 32 signal and thus the O_2 pressure in the system increases significantly and reversibly and the signal increase is proportional to the current I (Fig. 3b). Thus, under these conditions, the YSZ sample is losing nonstoichiometric oxygen, O(YSZ) at a rate $I/2F$, where I is the current generated by the applied potential and F is Faraday's constant. In view of the fact that YSZ is a pure O^{2-} conductor at temperatures below 1000 °C and O_2 pressures above 10^{-23} atm [70], it follows that the following reactions are taking place at the Pt (anode) and Au (cathode) electrodes during the experiments of Fig. 3:

$$O^{2-} \rightarrow \frac{1}{2}O_2(g) + 2e^- \quad \text{(anode)}, \tag{4}$$

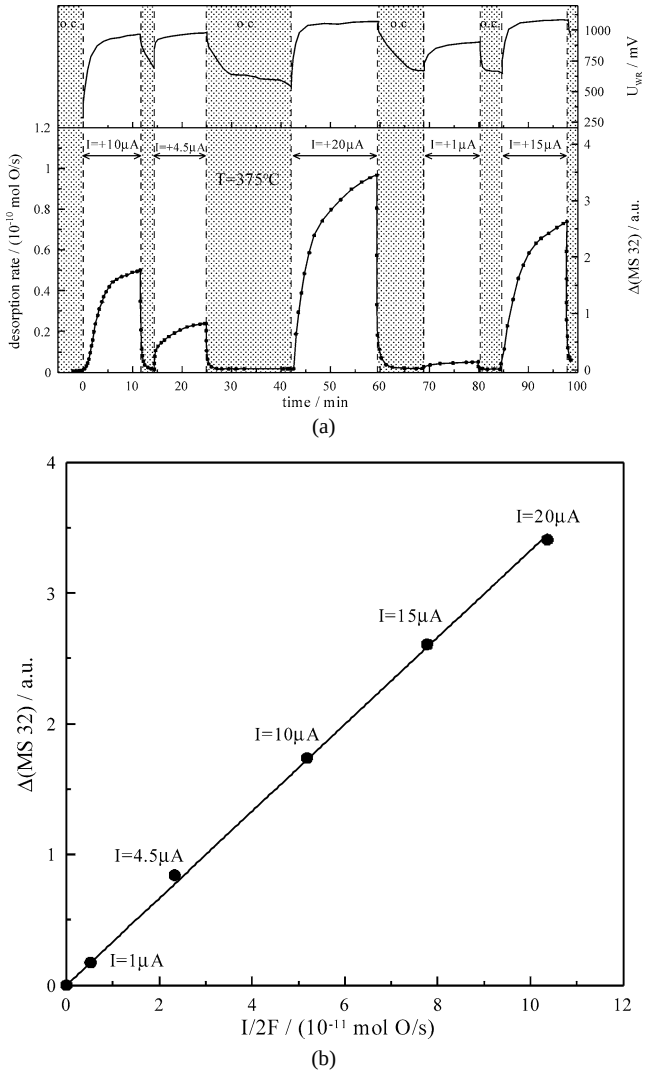

Fig. 3. (a) Variation of the MS 32 signal and concomitant O_2 desorption rate in the vacuum system upon application of constant currents ($I = 1$ to 20 μA) to the Pt/YSZ/Au sample at 375 °C. (b) Effect of applied current, I, and concomitant rate of $^{16}O^{2-}$ supply to the Pt catalyst ($I/2F$) on the increase of the $^{16}O_2$ signal in the vacuum system. This diagram was used to express all O_2 desorption rates in moles O/s.

$$O(YSZ) + 2e^- \rightarrow O^{2-} \quad \text{(cathode)}. \tag{5}$$

Consequently the $O_2(g)$ evolution taking place by reaction (4) is responsible for the observed reversible p_{O_2} increase (Fig. 3a). This Δp_{O_2} signal which depends only on the applied current, I, thus rate, $I/2F$, of O_2 evolution and on the pumping speed of the vacuum system can be used to calibrate all kinetic processes taking place in the vacuum system, (e.g., O_2 evolution), by comparing their MS signal with that corresponding to the measurable quantity $I/2F$ (mol O/s) (Fig. 3b).

When the applied current is maintained for long periods of time, then the nonstoichiometric oxygen-storage reservoir of YSZ is depleted (reaction (5)) and thus reaction (4) also stops. This is shown in Fig. 4 where the polarity of the applied potential between the Pt and Au (0.8 V) elec-

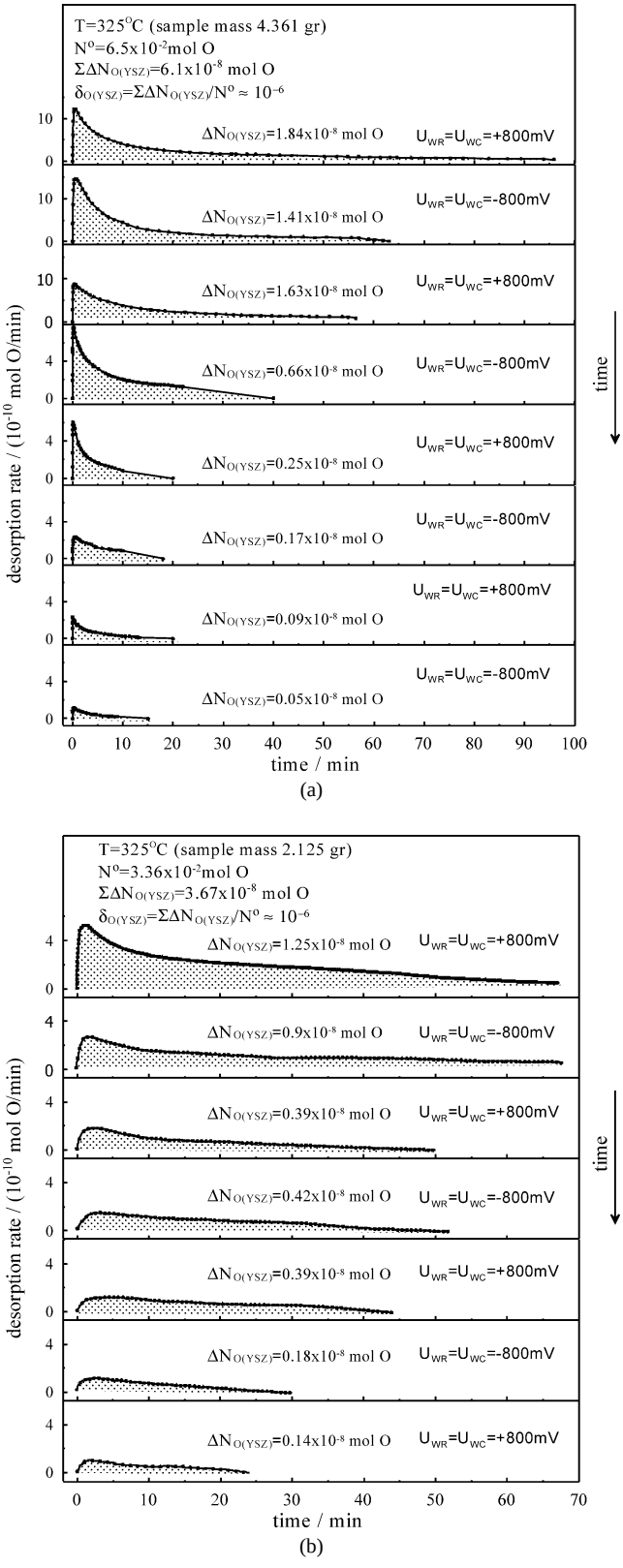

Fig. 4. Electrochemical removal of excess nonstoichiometric oxygen, O(YSZ), from the YSZ sample via successive application of positive and negative potentials (±0.8 V) between the Pt catalyst and the Au counterelectrode at 375 °C. (a) YSZ sample 1, YSZ mass 4.361 g, (b) YSZ sample 2, YSZ mass 2.125 g.

trodes has been reversed several times in order to speed up the electrochemical removal of O(YSZ) via reactions (4) and (5). By integrating the total area, $\Sigma\Delta N_{O(YSZ)}$, under the desorption rate vs t curves (Fig. 4) and dividing by the total mol of O, N^o, in the YSZ sample one can thus calculate the initial oxygen nonstoichiometry, $\delta_{O(YSZ)}$. The measured value of $\delta_{O(YSZ)} = 10^{-6}$ is in qualitative agreement with literature [68,69]. In general $\delta_{O(YSZ)} = \delta_{O(YSZ)}(a_{O_2}, T)$, where a_{O_2} is the activity of oxygen in the solid. The measured $\delta_{O(YSZ)}$ value can also be expressed in terms of oxygen-storage capacity (OSC) [54–57] and the corresponding value is 15.5×10^{-3} μmol O/g YSZ. Due to the fixed oxidation state of both Zr and Y in YSZ this value is four orders of magnitude smaller than the OSC of CeO_2 and $Ce_xZr_{(1-x)}O_2$ materials [54–57] where the large OSC is due to the Ce^{4+}/Ce^{3+} oxidation/reduction process [54–57].

At the final state of Fig. 4, the YSZ sample is at practically zero nonstoichiometric oxygen. If a fixed current is further applied, then the cell voltage exceeds the thermodynamic value of ∼ 2.3 V and reduction of YSZ (blackening) starts taking place at the Au cathode [14]. Consequently, the procedure shown in Figs. 3 and 4 can be used not only to calibrate the rate of kinetic processes in UHV systems, as described above (Fig. 3), but also to measure $\delta_{O(YSZ)}$ (Fig. 4). In these experiments care must be exercised so that the applied voltage, U_{WC}, between the working and the counterelectrodes does not exceed the YSZ electrolysis voltage of ∼ 2.3 V [14].

3.3. Interpretation of the O_2 TPD spectra of the Pt/YSZ system

The interpretation of the O_2 TPD spectra (Fig. 2) is strongly assisted by the observations discussed in the previous section. We present the interpretation of the TPD spectra of Fig. 2 here ($^{18}O_2$ adsorption on Pt/YSZ film *without* any previous current or potential application) in order to facilitate the understanding of the subsequent TPD results referring to $^{18}O_2$ TPD from the same electrochemically promoted Pt/YSZ film (Section 3.4) and from the nanodispersed Pt/YSZ powders (Section 3.5). The interpretation presented here applies equally well to these results (Sections 3.4 and 3.5) which can then be followed and understood thoroughly much easier.

We start by noting that $^{16}O_2$ desorption from the solid electrolyte can take place only when the oxygen excess, $\delta_{O(YSZ)}$, is larger than the $\delta_{O(YSZ)}$ value, denoted by $\delta_{O(YSZ)eq}(a_{O_2}, T)$ which corresponds to the equilibrium

$$O_2(g) \leftrightarrows 2O(YSZ), \tag{6}$$

i.e.,

$$\delta_{O(YSZ)} > \delta_{O(YSZ)eq}(a_{O_2}, T). \tag{7}$$

Thus, without any gaseous O_2 adsorption, $\delta_{O(YSZ)}$ is at the value corresponding to the a_{O_2} (or P_{O_2}) value of the vac-

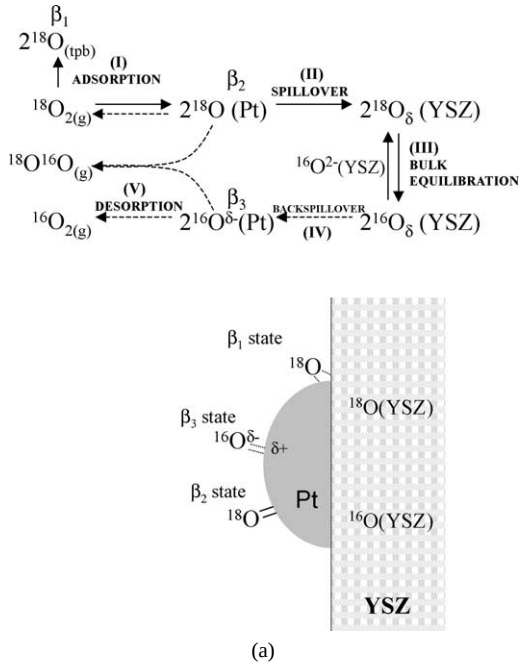

(a)

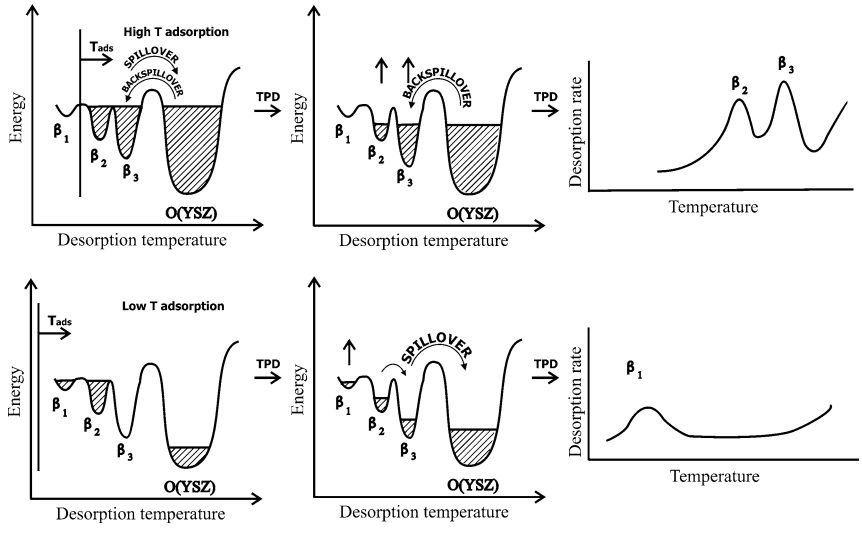

(b)

Fig. 5. (a) Top: Oxygen adsorption, spillover, bulk equilibration, backspillover, and desorption pathways of the Pt/YSZ system leading to the appearance of the β_1, β_2, and β_3 oxygen states. Pathways shown by solids arrows are active during O_2 adsorption; pathways shown by broken arrows are activated during desorption (TPD run). Bottom: Schematic of the location of the β_1, β_2, β_3, and O(YSZ) states. (b) Rationalization of the TPD spectra of Fig. 2a (top) and Fig. 2b (bottom) in terms of the approximate energy level and population diagram of the β_1, β_2, β_3 states (Pt surface) and of the O(YSZ) state (YSZ bulk).

uum system ($\sim 10^{-13}$ mbar); i.e., $\delta_{O(YSZ)}$ is very low and its desorption becomes thermodynamically possible only at very high temperatures ($> 540\,^{\circ}C$) as experimentally observed (Fig. 2).

When, however, gaseous $^{18}O_2$ adsorption takes place before the TPD run (e.g., at $P_{O_2} = 10^{-6}$ mbar, Fig. 2a), then during the adsorption period, $^{18}O_2$ adsorbs as atomic oxygen not only at the Pt/gas interface but also, via Pt-mediated spillover, forms additional excess nonstoichiometric oxygen, O(YSZ), according to reaction (6).

This excess oxygen $^{18}O(YSZ)$ can rapidly exchange with $^{16}O^{2-}$ in the YSZ lattice, so that the following equation holds:

$$\frac{^{18}O(YSZ)}{^{18}O(YSZ) + {}^{16}O(YSZ)} = \frac{^{18}O^{2-}}{^{18}O^{2-} + {}^{16}O^{2-}} \approx \varepsilon. \tag{8}$$

For the experiment of Fig. 2a (high-temperature $^{18}O_2$ adsorption), the increase in ε is of the order of 10^{-7}, as can be computed from the total $^{18}O_2$ uptake divided by the amount of $^{16}O_2$ in the YSZ lattice. Consequently, the enrichment with ^{18}O of the YSZ sample during $^{18}O_2$ adsorption preceding the TPD run is quite small for each TPD run and thus even after a few hundreds of TPD runs carried out in the present work, most of the desorbing lattice oxygen is $^{16}O_2$.

Fig. 5a shows schematically the O_2 adsorption, spillover, backspillover, and desorption pathways. Pathways shown by

solid arrows are active during adsorption; pathways shown by broken arrows are activated during desorption. Consequently, the dashed arrow pathways in Fig. 5a are activated only during the TPD run, i.e., upon heating the Pt/YSZ sample at elevated temperatures.

As already noted and as further discussed in Section 4, the low-temperature state β_1 can be assigned to O atoms adsorbed at the three-phase boundaries Pt–YSZ–gas. In agreement with the electrochemical promotion literature [14,46,47] and in full agreement with Fig. 2a, state β_2 is assigned to atomic O, originating from the gas phase and chemisorbed at the Pt/gas interface while state β_3 is assigned to backspillover anionic oxygen, $O^{\delta-}$ [14,46,47], migrating from the solid electrolyte to the Pt/gas interface.

As shown schematically in Fig. 5b the oxygen spillover step (II) of Fig. 5a requires temperatures of 200 °C or higher to be activated. At lower adsorption temperatures only step (I) takes place during the adsorption process, so that only $^{18}O_2$ (state β_1) desorbs in the TPD run (Fig. 5b).

Fig. 5b shows schematically the population of states β_1, β_2, and β_3, as well as of YSZ nonstoichiometric oxygen, O(YSZ), at the beginning of the TPD run, for the two cases of (top) high-T adsorption (activated spillover and thus equilibration of O adsorbed in states β_2, β_3 and in O(YSZ)) and (bottom) low-T adsorption (no spillover, thus occupancy only of states β_1 and β_2).

As shown in the middle and right section of Fig. 5b, in the former case (top, high-T adsorption) the oxygen adsorption states remain equilibrated during the TPD run and thus states β_2 and β_3 appear in the TPD spectrum.

In the latter case, however (bottom, low-T adsorption), state β_1 desorbs at low temperatures and during the TPD run the oxygen spillover process gets activated with a consequent migration of the oxygen initially populating the β_2 and β_3 states into the YSZ bulk and consequent disappearance of the β_2 and β_3 states from the TPD spectrum as experimentally observed (Fig. 2b). In general, all observations of Fig. 2 (and subsequent TPD figures) can be rationalized by the scheme of Fig. 5a in conjunction with Fig. 5b.

3.4. $^{18}O_2$ adsorption on the electrochemically promoted Pt/YSZ film

Fig. 6 shows O_2 TPD spectra of the Pt/YSZ film following high-temperature (275 °C) mixed gaseous–electrochemical O_2 adsorption, i.e., simulating conditions of electrochemical promotion. The Pt/YSZ film is first exposed to 2 kL of $^{18}O_2$ at $T_{ad} = 275$ °C for 45 min, followed by electrochemical supply of $^{16}O^{2-}$ at a rate $I/2F$ ($I = 15$ μA) for 210 s (total electrochemical supply of 1.63×10^{-8} mol O). As expected, this electrochemical $^{16}O^{2-}$ supply accelerates and fixes the rate of the backspillover step (III) (Fig. 5a) to the value of $I/2F$ and thus the anionic $^{16}O^{\delta-}$ backspillover peak in the TPD spectrum (state β_3) is enhanced (Fig. 6).

Fig. 6 also shows that some exchange of ^{18}O and ^{16}O is taking place between the β_2 and the β_3 state during the TPD

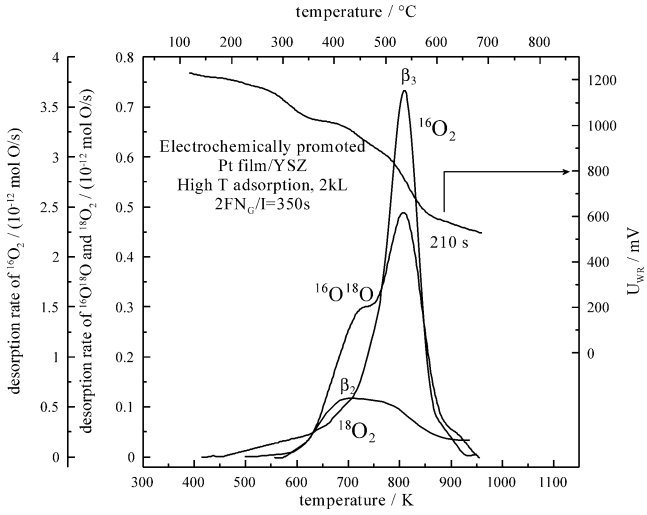

Fig. 6. Electrochemically promoted Pt/YSZ film, high-temperature adsorption: thermal desorption spectra after gaseous $^{18}O_2$ adsorption at 275 °C at $P_{^{18}O_2} = 10^{-6}$ mbar for 45 min (exposure 2 kL) followed by electrochemical $^{16}O^{2-}$ supply for 210 s with a constant current of +15 μA. Also shown is the catalyst potential, U_{WR}, variation during the TPD run. Desorption was performed with linear heating rate, $\beta = 0.5$ °C/s.

run, but this exchange is not rapid enough to obscure the origin of the two states. The significant presence of ^{16}O, in particular, in the β_2 state is well expected during a TPD run, since it is known from the electrochemical promotion literature [13,14], including recent STM observations [27], that state β_3 gets populated only when state β_2 is occupied. This explains why electrochemical promotion via O^{2-} supply is obtained only under oxidizing gas-phase compositions when using YSZ as the solid electrolyte [13,14]. Thus when $^{18}O_2$ desorbs from state β_2 during a TPD run, the resulting vacant surface sites can get rapidly populated again by lattice oxygen during the TPD transient, resulting in a significant presence of ^{16}O in the TPD spectrum of the β_2 state.

However, despite some isotopic scrambling and despite the above transient phenomenon, it is interesting to note the distinguishability of electrochemically supplied oxygen (^{16}O) and gas-phase-supplied oxygen (^{18}O) in Fig. 6. Previous $^{16}O_2$ TPD studies [45–47] have identified clearly the existence of two distinct O_2 desorption peaks on Pt/YSZ films subject to anodic polarization (electrochemical promotion) conditions (Fig. 7, which comes from Ref. [46]). In fact, Fig. 7 has served for several years as one of the basic observations for interpreting the molecular mechanism of electrochemical promotion [14].

Electrochemically supplied O^{2-} forms strongly bonded backspillover $O^{\delta-}$ species on the Pt/gas interface (peak β_3) which increase the Pt surface work function Φ [1] and act as sacrificial promoters [1,14] by forcing coadsorbed gas-supplied O(Pt) to a more weakly bonded state (peak β_2). The present work (Fig. 6) fully supports this molecular mechanism by confirming that on electrochemically promoted films the strongly bonded $O^{\delta-}$ peak β_3 corresponds to lat-

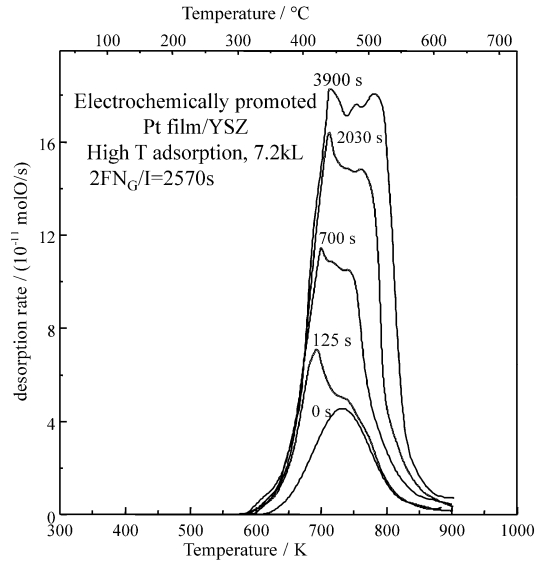

Fig. 7. Electrochemically promoted Pt/YSZ film, high-temperature adsorption [46]: thermal desorption spectra after gaseous normal oxygen adsorption at 400 °C and $P_{^{16}O_2} = 5.3 \times 10^{-6}$ mbar for 30 min (exposure 7.2 kL) followed by electrochemical $^{16}O^{2-}$ supply (+15 μA) for various time periods [46]. Desorption was performed with linear heating rate, $\beta = 1\,^{\circ}C/s$.

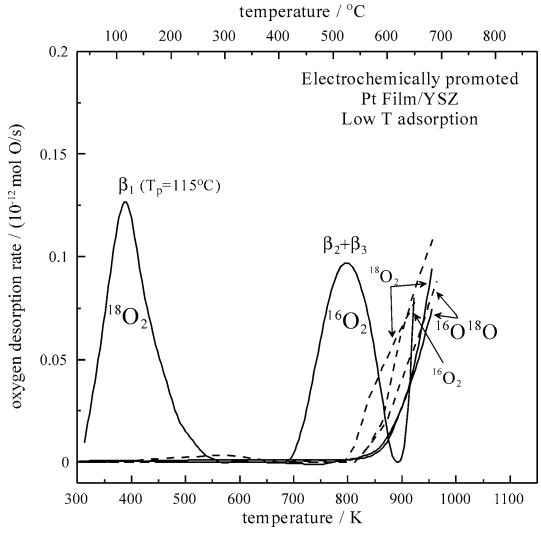

Fig. 8. Electrochemically promoted Pt/YSZ film, low-temperature adsorption: thermal desorption spectra after electrochemical supply of oxygen, $^{16}O^{2-}$, at 275 °C using a constant potential, $U_{WR} = +2$ V, followed by cooling under the applied potential and gaseous adsorption of $^{18}O_2$ at 70 °C. Desorption was performed with linear heating rate, $\beta = 0.5\,^{\circ}C/s$.

tice oxygen ($^{16}O^{\delta-}$) and the weakly bonded O peak β_2 to gas-supplied oxygen (^{18}O).

Fig. 8 also confirms the above molecular mechanism. Here electrochemical oxygen $^{16}O^{2-}$ supply was carried out first at 275 °C followed by cooling to 70 °C under applied positive bias and gaseous adsorption $^{18}O_2$ at 70 °C. It can be seen now that lattice oxygen ^{16}O has occupied both β_2 and β_3 states, which have merged into one state, and has forced gaseous oxygen (^{18}O) to occupy only the weakly bonded state β_1 which is now displaced at $T_p =$

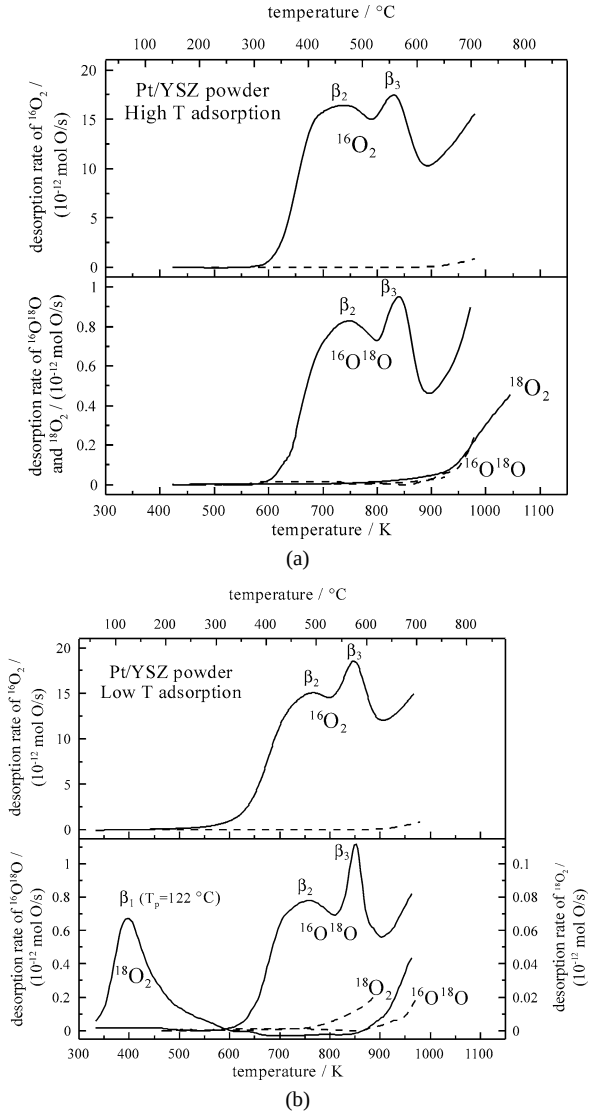

Fig. 9. Pt/YSZ powder: thermal desorption spectra from the nanodispersed Pt/YSZ catalyst (1% Pt/YSZ, $m = 140$ mg) after gaseous isotope oxygen dosing of 27 L ($P_{^{18}O_2} = 10^{-7}$ mbar for 6 min) at (a) 200 °C and (b) 70 °C. Dashed lines show spectra taken without any gaseous adsorption. Desorption was performed with linear heating rate, $\beta = 0.5\,^{\circ}C/s$.

115 °C vs $T_p \approx 157\,^{\circ}C$ obtained under open-circuit conditions (Fig. 2b). Both observations can be attributed to the strong repulsive lateral interactions between $^{16}O^{\delta-}$ and adsorbed ^{18}O [13,14,71]. These strong lateral interactions have been shown by rigorous ab initio quantum mechanical calculations [71] to be the key for rationalizing electrochemical promotion [13,14,71].

3.5. $^{18}O_2$ adsorption on nanodispersed Pt/YSZ catalysts

Figs. 9a and 9b show O_2 TPD spectra obtained under high vacuum conditions with the supported nanodispersed Pt/YSZ catalyst following $^{18}O_2$ adsorption at 200 and 70 °C, respectively.

The similarity of Fig. 6 with Fig. 9a and of Fig. 8 with Fig. 9b, respectively, is noteworthy. Figs. 6 and 8 correspond to the electropromoted Pt/YSZ film at high and low gas adsorption temperatures, respectively. Note that in the case of the nanodispersed Pt/YSZ catalyst (Fig. 9) the high-temperature adsorption peaks β_2 and β_3 are both occupied primarily by the lattice oxygen, even for low-temperature adsorption (Fig. 9b) and only the low-temperature adsorption peak β_1 is occupied by ^{18}O. The peak desorption temperature, T_p, of the β_1 peak ($T_p = 122\,^\circ C$, Fig. 9b) is very similar to that of the electropromoted Pt/YSZ film ($T_p = 115\,^\circ C$, Fig. 8).

The same information is conveyed by the TPD spectra of Figs. 10a and 10b which compare the spectra of Figs. 9a and 9b (bottom of the figures) with those (top of the figures) obtained with the same nanodispersed Pt/YSZ material sample at near *atmospheric* total pressure ($P_{^{18}O_2} = 2$ kPa) using the *same* Pt/YSZ-supported catalyst and the same adsorption temperatures as Figs. 9a and 9b, i.e., $T_{ad} = 200$ and $70\,^\circ C$. In this case, the Pt/YSZ catalyst was exposed to $P_{^{18}O_2} = 2$ kPa at $200\,^\circ C$ for 60 min (Fig. 10a) and to $P_{^{18}O_2} = 2$ kPa at $70\,^\circ C$ for 60 min (Fig. 10b), followed in both cases by flushing with ultrapure He for 120 s before starting the TPD run, again in flowing ultrapure He. Note the positive shift of peaks β_2 and β_3 in the case of atmospheric pressure TPD (Fig. 10b). This is to be expected due to the atmospheric pressure TPD conditions which allow for oxygen readsorption. Nevertheless, the conclusion is again the same as with high-vacuum TPD for the Pt/YSZ catalysts: The β_1 state is occupied by gaseous oxygen ($^{18}O_2$) while the β_2 and β_3 states are occupied primarily by ^{16}O via backspillover of lattice oxygen.

Figs. 11 and 12 provide a direct comparison of the high-vacuum O_2 TPD spectra of the nanodispersed Pt/YSZ catalyst and of the electrochemically promoted Pt/YSZ film. Fig. 11 refers to high-temperature adsorption ($T_{ads} = 200$ to $275\,^\circ C$) where only states β_2 and β_3 form. Fig. 11a shows the $^{16}O^{18}O$ TPD spectra. The similarity is striking and underscores the mechanistic equivalence of electrochemical promotion and metal–support interactions.

Fig. 11b presents the corresponding $^{16}O_2$ and $^{18}O_2$ TPD spectra. The figure, in conjunction with Fig. 11a, reveals the only mechanistic difference between electrochemical promotion and metal–support interactions: states β_2 and β_3 are present in both cases and state β_3 is always occupied by lattice oxygen. But state β_2 is occupied primarily by lattice oxygen (^{16}O) in the case of the supported nanodispersed catalyst and primarily by gaseous oxygen (^{18}O) in the case of the electrochemically promoted Pt/YSZ film. This difference, as well as the population of the β_2 and β_3 states by lattice oxygen even for low temperature adsorption (Figs. 9b, 10b, and 12), is reasonable in view of the very close (molecular distance) proximity of the surface of the Pt nanoparticles with the YSZ support in the case of the nanodispersed catalyst where the backspillover path of lattice oxygen is very short, i.e., of nanometer distances.

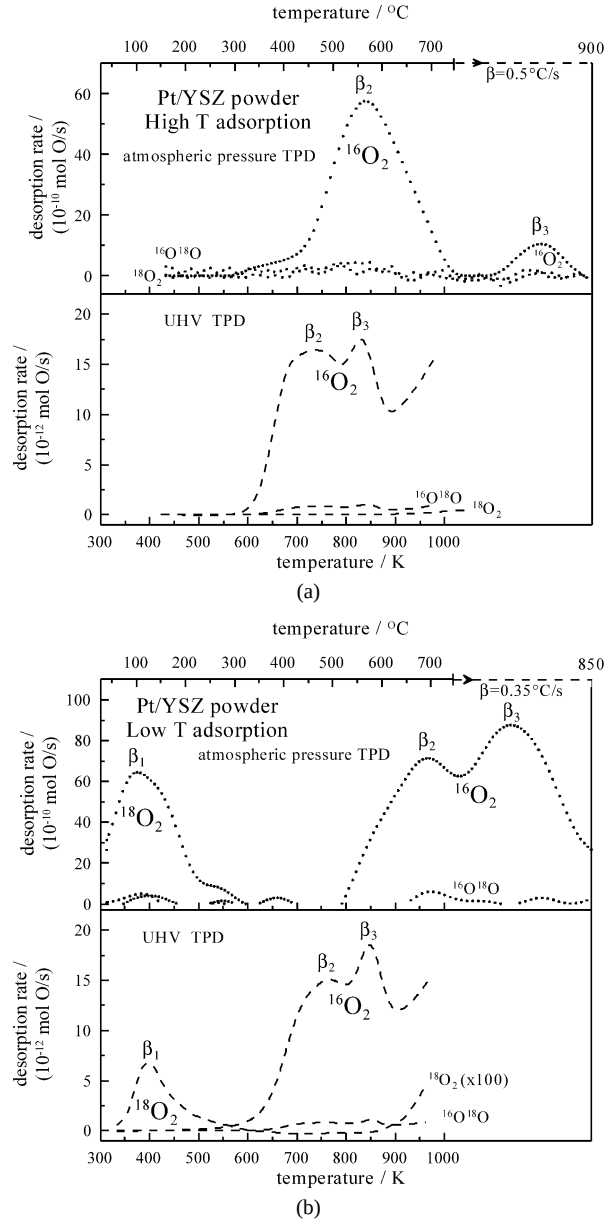

Fig. 10. Comparison of oxygen thermal desorption spectra from Pt-supported catalyst (1% Pt/YSZ) taken under UHV conditions (bottom, $P_{^{18}O_2} = 10^{-7}$ mbar, $t_{ads} = 6$ min, $m_{cat} = 140$ mg) and under atmospheric pressure (top, $P_{^{18}O_2} = 20$ mbar, $t_{ads} = 60$ min, $m_{cat} = 200$ mg) at high adsorption temperature $T_{ads} = 200\,^\circ C$ (a) and low adsorption temperature $T_{ads} = 70\,^\circ C$ (b). Heating rate, $\beta = 1.5\,^\circ C/s$ till $750\,^\circ C$ (top) and $\beta = 0.5\,^\circ C/s$ (bottom).

The same conclusions are reached from Fig. 12 which compares the O_2 TPD spectra of the nanodispersed Pt/YSZ catalyst obtained under UHV and at atmospheric pressure and of the electrochemically promoted Pt/YSZ film for low adsorption temperature ($T_{ads} = 70\,^\circ C$). In all cases the β_1 state is occupied by gaseous oxygen (^{18}O) while states β_2 and β_3 are occupied in all cases primarily by lattice oxygen. In the case of the Pt/YSZ film the β_2 and β_3 states have merged into one, apparently due to the long period of electrochemical supply of O^{2-} under anodic polarization.

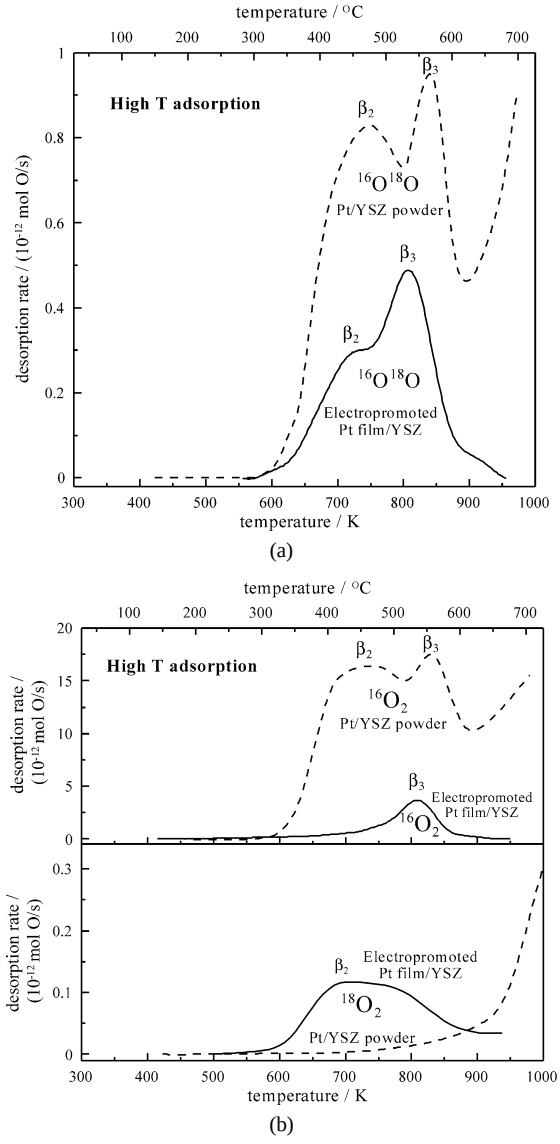

Fig. 11. Comparison of oxygen thermal desorption spectra from nanodispersed Pt/YSZ catalyst (1% Pt/YSZ) and from Pt/YSZ film taken under UHV conditions. (a) Comparison of $^{16}O^{18}O$ desorption; (b) comparison of desorption of $^{18}O_2$ and $^{16}O_2$. Desorption was performed with linear heating rate, $\beta = 0.5\,^{\circ}C/s$.

State β_1 requires some special attention since it is a state not formed on isolated Pt surfaces [31,43] or on isolated YSZ surfaces [14,46]. It results from the interaction of Pt and the YSZ and one can consider three possibilities:

(I) A surface YSZ adsorption state resulting from the interaction of YSZ with Pt.
(II) A surface Pt state resulting from the interaction of Pt with YSZ (and the concomitant $^{16}O^{\delta-}$ backspillover to the Pt surface).
(III) A state at the Pt/YSZ interface, i.e., at the Pt/YSZ/vacuum three-phase boundaries.

The third possibility is supported by the following observations:

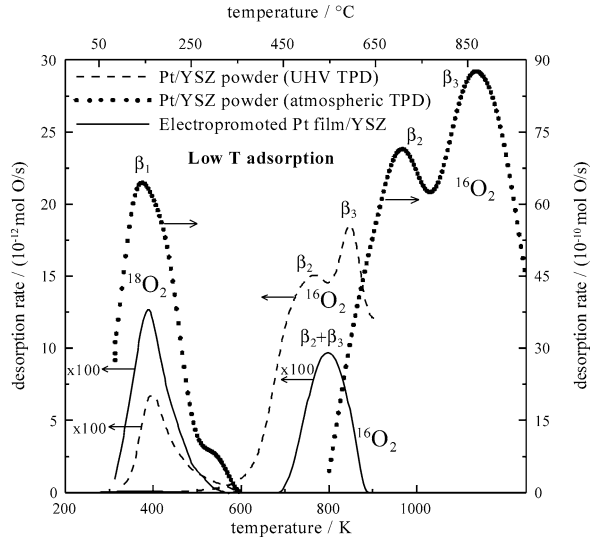

Fig. 12. Comparison of O_2 TPD spectra of the nanodispersed Pt/YSZ catalyst (UHV TPD and atmospheric pressure TPD) and of the electrochemically promoted Pt/YSZ film for low adsorption temperature, $T_{ad} = 70\,^{\circ}C$. Based on Figs. 8, 9b, and 10b. Heating rate $\beta = 0.5\,^{\circ}C/s$ for the film and the UHV powder TPD and $1.5\,^{\circ}C/s$ up to $750\,^{\circ}C$ followed by $0.35\,^{\circ}C$ above $750\,^{\circ}C$ for the atmospheric pressure power TPD.

(a) Similar states have been observed in our studies of Pt interfaced with other ionically conducting supports (CeO_2, W^{6+}-doped TiO_2, γ-Al_2O_3) [67].
(b) The *maximum* area of the β_1 peak typically accounts for 3% of the *maximum* combined β_2 plus β_3 peak areas in the case of the Pt/YSZ film (Fig. 2) and up to 30% of the *maximum* combined β_2 plus β_3 peak areas in the Pt/YSZ nanodispersed catalysts under atmospheric pressure TPD (Fig. 10b, top).

For the case of the low-temperature adsorption on the electropromoted film (Fig. 8), the area of state β_1 is larger than that of the merged $\beta_2 + \beta_3$ peaks but in this case the latter are very far from saturation. Also under UHV TPD conditions with the powder catalyst (Fig. 10b bottom and Fig. 12), state β_1 is again far from saturation (it did not approach saturation for O_2 exposures up to 27 L), and thus the TPD area of peak β_1 is only 0.3% of the sum of the areas of the β_2 and β_3 peaks. Thus it must be noted in the TPD comparison of Fig. 12 that the β_1 state of the Pt/YSZ powder under UHV TPD and the $\beta_2 + \beta_3$ states of the electropromoted film are both far from saturation.

In order to examine in some more detail if the assignment of state β_1 to oxygen adsorption at the tpb is consistent with the experimental results, one may consider the following simple model: Assuming semispherical Pt particles of diameter d in contact with YSZ, one computes that the ratio of the tpb sites, N_{tpb} to the Pt/gas sites, N_G, is given by

$$\frac{N_{tpb}}{N_G} = \frac{\pi d_{Pt}}{2d}, \tag{9}$$

where d is the diameter of the Pt particle and d_{Pt} is the diameter of the Pt atom in the particle (≈ 0.28 nm).

Using the same model to relate the metal dispersion, D_c, to the particle diameter, d, one obtains

$$D_c = 1/(1 + d/d_{Pt}). \quad (10)$$

One can apply these approximate expressions first to the film, then to the powder catalyst.

For the *film* one has $N_{tpb}/N_G = 2 \times 10^{-3}$, thus from Eq. (9) one obtains $d = 0.24$ μm and, from Eq. (10), $D_c = 1.16 \times 10^{-3}$, in good qualitative agreement with the value $D_c = 1.67 \times 10^{-3}$ computed from the Pt film surface area ($N_G = 2.7 \times 10^{-8}$ mol Pt). From this model one has $N_{tpb} = 4.9 \times 10^{-11}$ mol O while the maximum value for O adsorbed in the state β_1 is 3.3×10^{-11} mol O (Fig. 8).

For the *powder*, one has from Eq. (10) $d/d_{Pt} \approx 2$, thus from Eq. (9) $N_{tpb}/N_G \approx 0.75$. This value is reasonably close to the maximum value of 0.3 found for the ratio of the TPD areas of the β_1 state divided by the combined areas of the β_2 and β_3 states. This qualitative agreement between this simplistic semispherical particle model and experiment may be, to some extent, fortuitous, but nevertheless shows that the assignment of the β_1 state to O adsorbed at the three-phase boundaries (metal/gas/solid electrolyte) is not contradicted by any of the experimental facts. It is likely that the β_1 state is related to that reported by Primet and co-workers for Pt/Al_2O_3 and $Pt/Ba–Al_2O_3$ catalysts [52], although in that case the separation of the β_1 state from higher T_p states was not as complete as in the present case.

The present $^{18}O_2$-aided investigation of oxygen adsorption on electropromoted Pt/YSZ films and nanodispersed Pt/YSZ catalysts has shown clearly in both cases the important role played by lattice oxygen in the resulting TPD spectra. Since all the TPD spectra of this work were obtained after a specific pretreatment to remove oxygen adsorbed from the previous run (700 °C in vacuum for UHV TPD and 650 °C under H_2 for atmospheric TPD) which result to a partly oxygen-deficient YSZ at the beginning of the $^{18}O_2$-adsorption process, one may wonder to what extent the resulting O_2 TPD spectra are sensitive to the specific conditions of this reducing pretreatment and how relevant these TPD spectra are to "real life" atmospheric pressure catalytic oxidations on electropromoted films and dispersed catalysts.

In order to address this, two points must be emphasized. First that the reducing pretreatment is necessary to remove oxygen adsorbed on Pt from previous O_2 exposure and is of the same type one would use for an unsupported Pt catalyst to remove adsorbed oxygen before starting an O_2 adsorption and TPD experiment. The fact that this reducing pretreatment leads inevitably, as shown by the present results, to a partially oxygen-deficient YSZ support appears to be an intrinsic property of the Pt/YSZ system both under UHV and under atmospheric pressure conditions. Certainly the intensity of the reducing pretreatment can affect the resulting YSZ partial oxygen deficiency, but the nature and approximate peak desorption temperature of the resulting O_2 TPD peaks are not significantly altered as shown by a comparison of the UHV and atmospheric TPD spectra. One may therefore conclude that the relevance of the present O_2 TPD results to atmospheric pressure electrochemical promotion and metal–support interactions of oxidation reactions is the same with the relevance of O_2 TPD spectra on unsupported metal catalysts with atmospheric pressure oxidation catalysis on the same unsupported metal surfaces, i.e., quite high.

4. Conclusions

The main findings of the present work can be summarized as follows:

(1) The O_2 TPD behavior of both Pt/YSZ films and Pt/YSZ nanodispersed catalysts is qualitatively very similar, particularly when the Pt/YSZ films is polarized anodically (Figs. 10–12).

(2) Gaseous $^{18}O_2$ adsorption at adsorption temperatures, T_{ads}, below 100 °C leads, both on Pt/YSZ films and nanodispersed Pt/YSZ, to a single $^{18}O_2$ desorption peak at $T_p \approx$ 100–160 °C, i.e., much lower than the atomic O desorption peak on unsupported Pt [31–43] ($T_p \approx$ 420–650 °C) and much higher than the molecular O_2 desorption peak on unsupported Pt [31–43] ($T_p \approx -100$ °C). This oxygen adsorption state, labeled β_1 state, is catalytically very active at temperatures as low as 70 °C, as described elsewhere [67]. As discussed below, there is strong evidence that this O peak corresponds to oxygen dissociatively adsorbed at the three-phase boundaries Pt–YSZ–vacuum.

(3) Gaseous adsorption at T_{ads} higher than 200 °C leads, as expected, to the disappearance of the β_1 peak and to the appearance of the β_2 and β_3 peaks at $T_p \approx 425$ °C and $T_p \approx$ 500 °C, respectively, in agreement with previous work [46]. On the supported Pt/YSZ catalysts both states are occupied by lattice ^{16}O. On the Pt/YSZ film, state β_2 is occupied by gaseous oxygen, ^{18}O, and state β_3 is occupied by lattice oxygen, ^{16}O. Lattice oxygen can be forced to occupy state β_2 as well via anodic polarization, i.e., $^{16}O^{2-}$ supply to the catalyst. Under these conditions the electrochemically promoted Pt/YSZ film appears almost identical with the Pt/YSZ nanodispersed catalyst (Figs. 10 and 11).

(4) Both the Pt film and the nanodispersed Pt catalyst mediate, via O spillover and backspillover, respectively, the incorporation of gaseous $^{18}O_2$ into the YSZ lattice during gaseous adsorption and the desorption of lattice ^{16}O to the gas phase during the TPD runs.

(5) The excess oxygen, O(YSZ), in the YSZ lattice plays a key role in rationalizing the oxygen TPD spectra. During $^{18}O_2$ adsorption on the previously reduced (700 °C in vacuum for UHV conditions and 650 °C under H_2 for atmospheric conditions) Pt surface at temperatures above 200 °C, significant $^{18}O_2$ diffusion into the oxygen-deficient YSZ lattice is also taking place via ^{18}O spillover from the Pt catalyst to form O(YSZ).

(6) The β_3 state, which is always occupied by lattice oxygen and has been known for years [14,45–47] to be the electromigrating $O^{\delta-}$ species responsible for electrochemi-

cal promotion with YSZ supports [14,45–47], is also present in the nanodispersed supported Pt/YSZ catalysts (Figs. 9–12). This corroborates the mechanistic equivalence of electrochemical promotion and metal–support interactions with O^{2-}-conducting supports [14,26].

In general, all the features of the TPD spectra can be interpreted, at least qualitatively, by the scheme shown in Fig. 5. The promoting role of backspillover lattice oxygen, $^{16}O^{\delta-}$, i.e., state β_3, is also evidenced in all the TPD spectra where it appears (high-T adsorption), since its presence always coincides with a significant lowering of the T_p of states β_1 and β_2.

In summary, oxygen adsorption on electrochemically promoted Pt/YSZ films and on nanodispersed Pt/YSZ powders is almost identical when one accounts for the much shorter $O^{\delta-}$ backspillover pathway in the case of the powders. These observations corroborate the mechanistic equivalence of electrochemical promotion and metal–support interactions with YSZ supports.

Acknowledgments

We thank Dr. Susanne Brosda for the AC impedance characterization of the Pt/YSZ film and the EU SMART and Hellenic Secretariat of Research and Technology PENED and EPEAEK (Hellenic Ministry of Education) Programmes for financial support. We are also very thankful to our Reviewer 1 for his very thorough review and numerous very helpful suggestions.

References

[1] C.G. Vayenas, S. Bebelis, S. Ladas, Nature 343 (1990) 625.
[2] J. Pritchard, Nature 343 (1990) 592.
[3] R.M. Lambert, F. Williams, A. Palermo, M.S. Tikhov, Top. Catal. 13 (2000) 91.
[4] G. Foti, S. Wodiunig, C. Comninellis, Curr. Top. Electrochem. 7 (2001) 1.
[5] C.A. Cavalca, G.L. Haller, J. Catal. 177 (1998) 389.
[6] L. Ploense, M. Salazar, B. Gurau, E.S. Smotkin, J. Am. Chem. Soc. 119 (1997) 11550.
[7] P. Vernoux, F. Gaillard, L. Bultel, E. Siebert, M. Primet, J. Catal. 208 (2002) 412.
[8] I. Metcalfe, J. Catal. 199 (2001) 247;
I. Metcalfe, J. Catal. 199 (2001) 259.
[9] C. Sanchez, E. Leiva, in: W. Vielstich, H. Gasteiger, A. Lamm (Eds.), Handbook of Fuel Cells: Fundamentals, Technology and Applications, vol. 2, Wiley, England, 2003.
[10] G.-Q. Lu, A. Wieckowski, Curr. Opin. Colloid Interf. Sci. 5 (2000) 95.
[11] B. Grzybowska-Swierkosz, J. Haber, Annual Reports on the Progress of Chemistry, The Royal Society of Chemistry, Cambridge, 1994.
[12] J.O.M. Bockris, Z.S. Minevski, Electrochim. Acta 39 (1994) 1471.
[13] C.G. Vayenas, M.M. Jaksic, S. Bebelis, S.G. Neophytides, in: J.O.M. Bockris, B.E. Conway, R.E. White (Eds.), Modern Aspects of Electrochemistry, vol. 29, Kluwer Academic/Plenum, New York, 1996, p. 57.
[14] C.G. Vayenas, S. Bebelis, C. Pliangos, S. Brosda, D. Tsiplakides, Electrochemical Activation of Catalysis: Promotion, Electrochemical Promotion and Metal–Support Interactions, Kluwer Academic/Plenum, New York, 2001, references therein.
[15] A. Wieckowski, E. Savinova, C.G. Vayenas (Eds.), Catalysis and Electrocatalysis at Nanoparticles, Dekker, New York, 2003.
[16] L.L. Hegedus, R. Aris, A.T. Bell, M. Boudart, N.Y. Chen, B.C. Gates, W.O. Haag, G.A. Somorjai, J. Wei, Catalyst Design: Progress and Perspectives, Wiley, New York, 1987.
[17] M.C.J. Bradford, M.A. Vannice, Catal. Today 50 (1999) 87.
[18] S.J. Tauster, S.C. Fung, R.L. Garten, J. Am. Chem. Soc. 100 (1978) 170.
[19] G.L. Haller, D.E. Resasco, Adv. Catal. 36 (1989) 173.
[20] E.C. Akubuiro, X.E. Verykios, J. Catal. 103 (1987) 173;
E.C. Akubuiro, X.E. Verykios, J. Catal. 113 (1988) 106.
[21] X.E. Verykios, in: A. Wieckowski, E.R. Savinova, C.G. Vayenas (Eds.), Catalysis and Electrocatalysis at Nanoparticles Surfaces, Dekker, New York, 2003.
[22] M. Haruta, A. Ueda, S. Tsubota, R.M.T. Sanchez, Catal. Today 29 (1996) 443.
[23] B.L. Mojet, J.T. Miller, D.E. Ramaker, D.C. Konigsberger, J. Catal. 186 (1999) 373.
[24] R.J. Farrauto, C.H. Bartholomew, Fundamentals of Industrial Catalytic Processes, Chapman & Hall, London, 1997.
[25] S. Kuba, P. Lukinskas, R.K. Grasselli, B.C. Gates, H. Knoezinger, J. Catal. 216 (2003) 353.
[26] J. Nicole, D. Tsiplakides, C. Pliangos, X.E. Verykios, C. Comninellis, C.G. Vayenas, J. Catal. 204 (2001) 23.
[27] C. Vayenas, D. Archonta, D. Tsiplakides, J. Electroanal. Chem. 554–555 (2003) 301.
[28] C. Pliangos, I.V. Yentekakis, V.G. Papadakis, C.G. Vayenas, X.E. Verykios, Appl. Catal. B 14 (1997) 161.
[29] C.G. Vayenas, G. Pitselis, I&EC Res. 40 (2001) 4209.
[30] C.G. Vayenas, S. Brosda, C. Pliangos, J. Catal. 216 (2003) 487.
[31] M.A. Barteau, E.I. Ko, R.J. Madix, Surf. Sci. 102 (1981) 99.
[32] M.T. Paffet, C.T. Campbell, G. Windham, B.E. Koel, Surf. Sci. 207 (1989) 274.
[33] A. Winkler, X. Guo, H.R. Siddiqui, P.L. Hagans, J.T. Yates, Surf. Sci. 201 (1988) 419.
[34] Y. Ohno, T. Matsushima, Surf. Sci. 241 (1991) 47.
[35] C.T. Campbell, G. Ertl, H. Kuipers, J. Segner, Surf. Sci. 107 (1981) 220.
[36] M. Sander, R. Imbihl, R. Schuster, J.V. Barth, G. Ertl, Surf. Sci. 271 (1992) 159.
[37] M.A. Weibel, K.M. Backstrand, T.J. Curtiss, Surf. Sci. 444 (2000) 66.
[38] H. Steininger, S. Lehwald, H. Ibach, Surf. Sci. 123 (1982) 1.
[39] P.R. Norton, K. Griffiths, P.E. Bindner, Surf. Sci. 138 (1984) 125.
[40] J.L. Gland, Surf. Sci. 93 (1980) 487.
[41] J.L. Gland, B.A. Sexton, G.B. Fisher, Surf. Sci. 95 (1980) 587.
[42] A.A. Gee, B.E. Haiden, Surf. Sci. 113 (2000) 10333.
[43] A.N. Artsyukhovich, V.A. Ukraintsev, I. Harrison, Surf. Sci. 347 (1996) 303.
[44] P.R. Norton, Surf. Sci. 47 (1975) 98.
[45] S.G. Neophytides, C.G. Vayenas, J. Phys. Chem. 99 (1995) 17063.
[46] S. Neophytides, D. Tsiplakides, C.G. Vayenas, J. Catal. 178 (1998) 414.
[47] D. Tsiplakides, S. Neophytides, C.G. Vayenas, Solid State Ionics 136–137 (2000) 839.
[48] W. Huang, Z. Jiang, J. Jiao, D. Tan, R. Zhai, X. Bao, Surf. Sci. 506 (2002) 287.
[49] C. Hwang, C. Yen, J. Mol. Catal. A 112 (1996) 295.
[50] E.S. Putna, J.M. Vohs, R.J. Gorte, Surf. Sci. Lett. 391 (1997) L1178.
[51] D. Uner, N.A. Tapan, I. Ozen, M. Uner, Appl. Catal. A 251 (2003) 225.
[52] V. Labalme, N. Guilhaume, E. Garhowski, M. Primet, React. Kinet. Catal. Lett. 64 (1998) 207.
[53] A. Mitterdorfer, L.J. Gauckler, Solid State Ionics 117 (1999) 203.
[54] Y. Madier, C. Descorme, A.M.L. Govic, D. Duprez, J. Phys. Chem. 103 (1999) 10999.
[55] A. Holmgren, D. Duprez, B. Andersson, J. Catal. 182 (1999) 441.
[56] S. Bedrane, C. Descorme, D. Duprez, Catal. Today 75 (2002) 401.

[57] C. Descorme, Y. Madier, D. Duprez, J. Catal. 196 (2000) 167.
[58] M. de Ridder, A.G.J. Vervoort, R.G. van Welzenis, H.H. Brongersma, Solid State Ionics 156 (2003) 255.
[59] M. de Ridder, R.G. van Welzenis, H.H. Brongersma, U. Kreissig, Solid State Ionics 158 (2003) 67.
[60] J.A. Kilner, Solid State Ionics 129 (2000) 13.
[61] J. Au-Yeung, A.T. Bell, E. Iglesia, J. Catal. 185 (1999) 213.
[62] D.K. Liguras, D.I. Kondarides, X.E. Verykios, Appl. Catal. B 43 (2003) 345.
[63] J.O. Hernandez, E.A. Choren, Thermochim. Acta 71 (1983) 265.
[64] A. Kotsifa, T.I. Halkides, D.I. Kondarides, X.E. Verykios, Catal. Lett. 79 (2002) 113.
[65] D. Tsiplakides, S. Neophytides, C.G. Vayenas, Ionics 7 (2001) 203.
[66] A.M. Efstathiou, D. Papageorgiou, X.E. Verykios, J. Catal. 141 (1993) 612.
[67] A. Katsaounis, T. Halkides, X.E. Verykios, C.G. Vayenas, J. Catal. (2003), submitted for publication.
[68] J. Xue, R. Dieckmann, Solid State Ionics 73 (1994) 273.
[69] R. Dieckmann, J. Phys. Chem. Solids 59 (1998) 507.
[70] J. Maier, Festkoerper—Fehler und Funktion: Prinzipien der Physikalischen Festkoerperchemie, Teubner, Stuttgart, 2000, references therein.
[71] G. Pacchioni, F. Illas, S. Neophytides, C.G. Vayenas, J. Phys. Chem. 100 (1996) 16653.